Thermal and Solvent Effects On NMR Indirect Spin-Spin Coupling Constants of a Prototypical Chagas Disease Drug

ARTICLE *in* THE JOURNAL OF PHYSICAL CHEMISTRY A · NOVEMBER 2011

Impact Factor: 2.69 · DOI: 10.1021/jp201576u · Source: PubMed

3 AUTHORS, INCLUDING:

Teodorico C. Ramalho
Universidade Federal de Lavras (UFLA)
188 PUBLICATIONS **1,684** CITATIONS

THE JOURNAL OF PHYSICAL CHEMISTRY A

ARTICLE

pubs.acs.org/JPCA

Thermal and Solvent Effects On NMR Indirect Spin−Spin Coupling Constants of a Prototypical Chagas Disease Drug

Teodorico C. Ramalho,*[,†] Douglas H. Pereira,[†] and Walter Thiel[‡]

[†]Department of Chemistry, Federal University of Lavras, 37200-000 Lavras, Minas Gerais, Brazil

[‡]Max-Planck-Institut für Kohlenforschung, Kaiser-Wilhelm-Platz 1, D 45470 Mülheim an der Ruhr, Germany

ABSTRACT: NMR *J*-couplings across hydrogen bonds reflect the static and dynamic character of hydrogen bonding. They are affected by thermal and solvent effects and can therefore be used to probe such effects. We have applied density functional theory (DFT) to compute the NMR ^{n}J(N,H) scalar couplings of a prototypical Chagas disease drug (metronidazole). The calculations were done for the molecule in vacuo, in microsolvated cluster models with one or few water molecules, in snapshots obtained from molecular dynamics simulations with explicit water solvent, and in a polarizable dielectric continuum. Hyperconjugative and electrostatic effects on spin−spin coupling constants were assessed through DFT calculations using natural bond orbital (NBO) analysis and atoms in molecules (AIM) theory. In the calculations with explicit solvent molecules, special attention was given to the nature of the hydrogen bonds formed with the solvent molecules. The results highlight the importance of properly incorporating thermal and solvent effects into NMR calculations in the condensed phase.

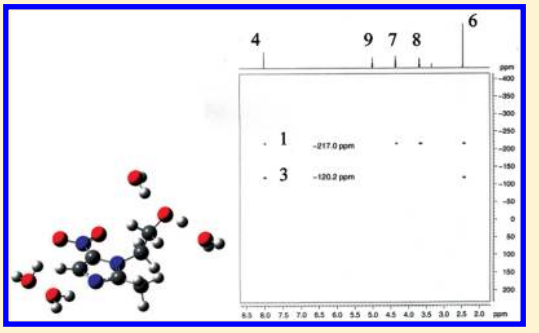

1. INTRODUCTION

Depite recent progress, Chagas disease is still one of the most serious health problems facing humanity, causing many deaths and having a great and limiting influence on the quality of life in many countries.[1−5]

To date, no single drug has been developed that is both readily absorbed and effective for an extended period.[1] The most promising drugs available are nitroimidazole and nitrofuran compounds.[6]

Therefore, the intracellular generation of free radicals appears to be a strategy that is exploited in the Chagas treatment with nitroimidazole and nitrofuran derivatives.[7] These electrophilic compounds behave as oxygen-mimicking species, affecting the *T. cruzi* cells and inducing damage to DNA and other molecules.[8−10] In practice, nitroimidazoles are used most, with metronidazole (**1**) (Figure 1) being considered a prototypical representative of that class.[1−8]

Recently, ^{1}H, ^{31}P, and ^{19}F NMR imaging[11] of nitroimidazoles has been applied for measuring tumor[12] and tissue oxygenation.[13] Other nitroimidazoles labeled with ^{19}F or ^{123}I have been investigated as possible noninvasive markers of hypoxia.[12−14]

In solution, the bioactive conformation of these drugs is most frequently studied by NMR spectroscopy through analysis of homo- and heteronuclear NMR spin−spin coupling constants (SSCC).[15,16] The theoretical calculation of SSCC values is challenging because the results may strongly depend on the molecular structure as well as on dynamics and solvent effects.[17,18] It is well-known that nonbonded electrons can strongly influence the SSCC values.[19] Experimentally, spin−spin coupling is crucial for indirect NMR detection techniques that are based on the transfer of magnetization from a more sensitive nucleus (usually a proton)

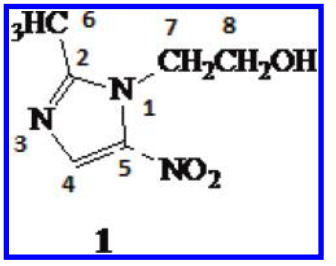

Figure 1. Structure and numbering of metronidazole.

to a heteronucleus.[20] Thermal and solvent effects on the SSCC of drugs such as **1** have not yet been measured, and surprisingly little computational work on the subject has appeared. Given the size of these systems, the most promising computational approach is to use density functional theory (DFT), which has been employed with success to reliably predict the chemical shifts of large compounds and complexes[21] because of the efficient incorporation of electronic correlation and relativistic effects.[22]

In fact, NMR signals primarily reflect local perturbations to electronic shielding (chemical shifts), short-range through-bond interactions (*J*-coupling), and medium-range through-space interactions (nuclear Overhauser effect). Hence, NMR spectroscopy is a technique sensitive to local conformation[23−29] that can be used for structure determination.[30−33] Our previous studies addressed ^{1}H, ^{13}C, and ^{15}N chemical shift calculations

Received: February 17, 2011
Revised: October 9, 2011
Published: October 13, 2011

on bioreductive drugs in solution and their electronic properties.[20,34] They showed the validity of the theoretical methodology used presently. Now, in the current work, we focus on the thermal and solvent contributions to the SSCC values of one such prototypical drug in the condensed phase because the coupling constants may be suitable to probe its behavior in solution. NMR experiments are generally conducted in polar solvents and at ambient temperature; therefore, it may be important to include thermal and solvent effects for reliable theoretical predictions.

The goal of the present study is to predict the spin−spin coupling constants for metronidazole (**1**) in solution using modern computational tools and giving special attention to thermal and solvent effects.

2. METHODOLOGY

2.1. Optimization Procedure and Molecular Dynamics Simulations. Geometries were fully optimized using the hybrid B3LYP density functional[35−38] and the 6-311++G**basis set, either in vacuo or in the presence of a polarizable continuum model[39−42] using the dielectric constant of water [denoted PCM(H_2O)]. The initial optimization of **1** was started from the coordinates taken from the solid-state structure.[20,43]

Molecular dynamics (MD) simulations were performed using the atom-centered density matrix propagation (ADMP) method at the DFT level.[44] Because the time scale accessible to such first-principles MD runs is very limited, no extensive equilibration is possible, and care must be taken to start from reasonably well pre-equilibrated configurations. To this end, we first prepared the system through a classical MD simulation using the force field GROMOS96 and the program GROMACS 4.0.[45] Periodic boundary conditions (PBC) and a cutoff distance of 9.0 Å were applied.[46] The substrate **1** was embedded in an array of 37 TIP3P water molecules in a cubic cell with a side of 11.0 Å. The initial configuration was minimized using the steepest descent and the conjugate gradient algorithm until the energy gradient was below 0.01 kcal mol^{-1} $Å^{-1}$. The subsequent MD simulation was performed at 300 K in a *NVT* (canonical) ensemble. It consisted of a thermalization stage of 1 ns, followed by an additional period of 2 ns, which was sufficient for complete equilibration. Using the last configuration from the classical MD as the starting point, we performed a B3LYP/6-31G** MD simulation using the ADMP method.[44] From the AIMD simulation, we have selected the solvent molecules based on geometric criteria to include in the NMR computations. This computational procedure has been used for similar systems with good results.[20,46−48] The calculations were carried out using Gaussian 09. After an equilibration time of 0.3 ps, in which a temperature of 300 K was maintained via velocity rescaling, statistical averages and snapshots for the NMR calculations were collected from subsequent unconstrained microcanonical runs of 1 ps. Snapshots were taken every 25 fs for use in the NMR calculations.

2.2. NMR Calculations. SSCC were computed at the GIAO (gauge-including atomic orbitals) level,[48−51] both for the optimized equilibrium geometries and for the snapshots taken from the MD simulations. These calculations employed the B3LYP functional and the EPR-III basis set[52] for the solute and for any explicitly included water molecules. They were carried out using Gaussian 09.[53]

The approach used presently has been shown to yield results comparable to more sophisticated correlated ab initio calculations or perturbation models.[15] Concerning the choice of the basis set, the performance of EPR-III was found to be acceptable in initial test calculations, consistent with previous experience.[15,17] Smaller basis sets were less satisfactory, and larger ones were more expensive without offering much higher accuracy.

2.3. AIM Topological Parameters and NBO Analysis. The topological properties of hydrogen bonds between solute and solvent were characterized at the B3LYP/6-311++G** level using the AIM theory of Bader.[54−59] The participation of nonbonded electrons was assessed through NBO analysis[60] at the same level, using the AIMALL[61] program and the AIM2000 visualization tool. Electrostatic charges were determined so as to reproduce the B3LYP/6-311++G** electrostatic potential (MEP).[62]

2.4. NMR Spectroscopy. Metronidazole was supplied by Rhodia Laboratories and by the Pharmacy Department, University of Sao Paulo (USP).[20] The SSCC between ^{1}H and ^{15}N were recorded under standard conditions on a Bruker DMX 600 spectrometer equipped with a cryoprobe, using ∼1.0 M samples in DMSO-d_6 using the HR-HMBC.[63]

3. RESULTS AND DISCUSSION

3.1. Indirect Detection techniques and SSCC values. Among the nitroimidazole-based drugs, metronidazole (**1**) is a prototypical representative, which has been widely used in the treatment of anaerobic protozoan and bacterial infections.[1,64] We therefore chose this molecule as the target for extensive tests of the methods available for computation of NMR properties, with emphasis on the SSCC values in the five-membered heterocyclic imidazole ring. The results in Table 1 show, as expected, that ^2J(N,H) is generally higher than ^3J(N,H). The highest SSCC values are found for ^2J(N-3,H-4) followed by ^3J(N-1,H-8) and ^3J(N-1,H-4). In previous experimental work, the ^{15}N chemical shifts were detected indirectly via ^{1}H using the HMBC (heteronuclear multiple bond correlation) protocol.[65] Such indirect detection techniques are based on the transfer of magnetization from a more sensitive nucleus, a proton in our case, to the heteronucleus of interest.[65] A prerequisite for this kind of approach is that both nuclei need to be involved in detectable (if not necessarily resolvable) mutual indirect spin−spin coupling, which actually marks the limitation of this technique; ^{15}N nuclei that are only weakly coupled to protons elsewhere in the molecule cannot be detected.[65] We note, in this context, that the theoretical SSCC values involving the nitro group (NO_2) are smallest, on average, about 0.14 Hz in absolute value (Table 1), and hence, such weak couplings may be hard to identify in the spectra.

The N-3 signal in the experimental HMBC spectrum[20] of **1** (Figure 2) is caused by the coupling between N-1 and H-4.[20] The N-1 signal is due to the coupling of N-1 with both H-4 and H-7. The nitro group is not detected in the HMBC spectrum, indicating indeed very small coupling with the hydrogen nuclei at the imidazole ring (below 1 Hz). The employed HBMC technique is not able to detect SSCC values smaller than 1 Hz and does not quantify the observed heteronuclear ^nJ(N,H) couplings.[65]

It is important to keep in mind, however, that the qualitative information on NMR *J*-coupling from the HMBC spectrum is not enough to map the thermal and solvent effects on SSCC values. Therefore, to obtain the ^nJ(N,H) SSCC values, we have used the HR-HMBC procedure.[63] This is a new method for measuring heteronuclear long-range coupling constants in complicated spin systems. To our knowledge, the spin−spin NMR spectroscopic characterization of **1** has not been complete, and

Table 1. ^2J(N,H) and ^3J(N,H) Spin−Spin Coupling Constants [Hz] for Metronidazole (1) Computed at the GIAO-B3LYP/EPR-III Level

level of approximation[a]	^2J(N-1,H-7)	^3J(N-1,H-4)	^3J(N-1,H-6)	^3J(N-1,H-8)	^2J(N-3,H-4)	^3J(N-3,H-6)	^3J(NO$_2$,H-4)
J_e(//B3LYP)	1.66	1.56	1.01	3.03	5.20	0.82	−0.14
J_e(PCM//B3LYP/PCM)	1.68	1.55	1.03	3.06	7.14	1.92	−0.15
J_e(B3LYP(1w))//B3LYP(1w))	1.73	1.61	1.12	3.09	7.31	2.15	−0.11
J^{300K}(//AIMD)	1.53 ± 0.53	1.41 ± 0.27	0.89 ± 0.51	2.93 ± 0.49	7.22 ± 0.64	2.03 ± 0.29	−0.15 ± 0.04
J^{300K}(AIMD/(PCM)//AIMD)	1.56 ± 0.48	1.47 ± 0.25	0.91 ± 0.49	2.99 ± 0.47	7.29 ± 0.65	1.93 ± 0.23	−0.13 ± 0.03
J^{300K}(AIMD(1w))//AIMD(1w))	1.55 ± 0.46	1.46 ± 0.21	0.89 ± 0.48	2.97 ± 0.48	7.86 ± 0.68	2.34 ± 0.27	−0.07 ± 0.05
J^{300K}(AIMD(H$_2$O)//AIMD(H$_2$O)[b])	1.59 ± 0.46	1.48 ± 0.23	0.94 ± 0.42	3.00 ± 0.40	7.62 ± 0.61	2.23 ± 0.19	−0.25 ± 0.07
J^{300K}(AIMD(H$_2$O)[b]/PCM//AIMD(H$_2$O)[b])	1.53 ± 0.44	1.43 ± 0.20	0.88 ± 0.44	2.95 ± 0.42	7.75 ± 0.63	2.16 ± 0.21	−0.10 ± 0.05
J Experimental	1.0 ± 0.3	1.7 ± 0.2	1.6 ± 0.3	3.3 ± 0.2	9.7 ± 0.2	1.9 ± 0.2	

[a] Notation: level of chemical shift computation//level of geometry optimization or MD simulation. [b] Section from the full solution containing seven water molecules explicitly (see text).

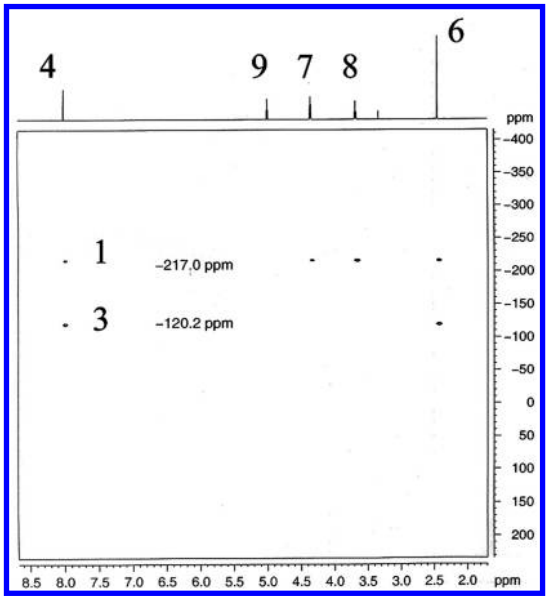

Figure 2. Experimental HMBC spectrum for **1** from ref 20.

those results may be useful to understand the coupling pathway at the imidazole ring. From Table 1, ^2J(N-1,H-7), ^3J(N-1,H-4), ^3J(N-1,H-6), and ^3J(N-3,H-6) are small (1.0−1.9 Hz). By contrast, the SSCC values for ^3J(N-1,H-8) and ^3J(N-3,H-4) are higher, about 3.3 and 9.7 Hz, respectively. It is important to mention that the spin−spin coupling constant between the nitro group and hydrogen 4 (^3J(NO$_2$,H-4)) was not detected. As predicted by theoretical calculations, the appreciable coupling with H-4 modulates the N-1 and N-3 NMR signals in the heterocyclic ring, while there is no detectable effect on the NO$_2$ NMR signal.

Those experimental results are in very good agreement with previously reported ^{15}N NMR chemical shift[20] and HMBC spectrum (Figure 2) for **1**. Overall, the experimental HR-HMBC results are thus in full qualitative accord with our theoretical results (Table 1).

3.2. Thermal and Solvent Effects. To gain deeper insight into the factors that influence the coupling pathway of **1** in solution, we investigated thermal and solvent effects. The latter can be treated by continuum models,[66] discrete cluster models, and explicit representations of the bulk solvent with the use of molecular dynamics. Each approach has its advantages and drawbacks, and careful validation is necessary in order to identify a particular method (or a combination thereof) that affords reliable results. In this paper, we assess these methods for the ^nJ(N,H) calculations of the prototypical Chagas disease drug **1**.

First, focusing on the structural parameters (Table 2), we do not find significant effects of the surrounding continuum; upon going from gas to solution phase, there is a slight decrease in the bond lengths N-1—C-2, N-1—C-5, and N-3—C-4, and a slight increase in N-3—C-2 [compare r_e(//B3LYP) and r_e(//B3LYP/PCM)]. Including thermal effects causes changes of 0.006, 0.002, −0.007, and −0.001 Å for N-1—C-2, N-1—C-5, N-3—C-4, and N-3—C-5, respectively [compare r_e(//B3LYP) and r^{300K}(//AIMD)]. When both thermal and solvent effects are introduced, the corresponding changes are 0.007, −0.002, −0.009, and 0.012 Å [compare r_e(//B3LYP) and r^{300K}(//AIMD(H$_2$O))]. On average, the deviation between the theoretical and the experimental solid-state results is 0.022, 0.017, 0.014, and 0.002 Å for these four bond lengths, respectively.

Next, we discuss the heteronuclear NMR SSCC of metronidazole (**1**) (Table 1). In five cases, there are no significant differences in the SSCC values computed at the structures optimized in vacuo and with the PCM continuum solvation model; both approaches agree within 0.03 Hz and yield ∼1.66, 1.56, 1.01, 3.03, and −0.14 Hz for ^2J(N-1,H-7), ^3J(N-1,H-4), ^3J(N-1,H-6), ^3J(N-1,H-8), and ^3J(NO$_2$,H-4), respectively. By contrast, the SSCC values for ^3J(N-3,H-4) and ^3J(N-3,H-6) increase by 1.94 and 1.10 Hz, respectively, when going from the gas phase to solution [compare J_e(//B3LYP) and J_e(PCM//B3LYP/PCM)], which corresponds to changes of 37 and 77%. Obviously, the N-3 atom is more sensitive to solvent effects. The presence of a lone pair adjacent to the unsaturated bonds at N-3 gives rise to a small energy gap between magnetically coupled molecular orbitals (MOs), thus producing large paramagnetic contributions to the magnetic shielding constant of this nucleus,[67−70] and it is usually these paramagnetic contributions that are sensitive to structural and electronic effects.

As a continuum approach, we used the well-known PCM. This method has the advantages over earlier, simpler variants in that the cavity is not limited to spherical or ellipsoidal cases but has a realistic shape and that the electrostatic problem is solved exactly without resorting to truncated multipolar expansions.

The lone pair at the N-3 atom can undergo specific interactions with the solvent, by acting as a hydrogen-bond acceptor. This cannot be realistically described by the PCM approach. As an alternative, discrete solvent molecules may be included in the

Table 2. Optimized (r_e) or Averaged (r^{300K}) Bond Lengths [Å] for Metronidazole (1)

level of approximation	N1—C2	N1—C5	N1—C10	N3—C2	N3—C4	C4—C5	C2—C9	C5—N6
r_e(//B3LYP)	1.378	1.400	1.476	1.343	1.363	1.391	1.496	1.432
r_e(//B3LYP/PCM(H_2O))	1.371	1.400	1.478	1.351	1.364	1.395	1.492	1.421
r_e(//B3LYP(1w))	1.373	1.400	1.476	1.349	1.364	1.388	1.494	1.433
r^{300K}(//AIMD)	1.381	1.406	1.483	1.345	1.365	1.391	1.498	1.433
r^{300K}(//AIMD/1w)	1.379	1.401	1.482	1.349	1.365	1.388	1.496	1.437
r^{300K}(//AIMD(H_2O))	1.371	1.402	1.487	1.353	1.351	1.397	1.488	1.405
r Experimental[a]	1.353(2)	1.384(9)	1.476(2)	1.334(2)	1.360(1)	1.337(5)	1.482(1)	1.417(8)

[a] From ref 30. Experimental error bars given in parentheses.

DFT calculations. In a first model, we considered **1** with one explicit water molecule bound to N-3, denoted (1w) in Table 1. Qualitatively, the solvent effects on ^2J(N-1,H-7), ^3J(N-1,H-4), ^3J(N-1,H-6), ^3J(N-1,H-8), and ^3J(NO_2,H-4) remain small (increase by 0.03−0.09 Hz), while those for ^2J(N-3,H-4) and ^3J(N-3,H-6) are again larger (increase by 2.11 and 1.33 Hz, or 41 and 93%, respectively) [see J_e(//B3LYP) and J_e(B3LYP(1w))//B3LYP(1w))]. Compared with the PCM results, the solvent effects from this model (1w) are generally slightly larger but qualitatively similar.

Thermal effects can be included by performing MD simulations of the solute in a box of explicit solvent molecules. One option would be to use classical force fields for this purpose. Most of these employ fixed atomic charges and thus neglect polarization effects. While polarizable force fields have been introduced in recent years,[68,69] a more accurate approach is offered by the technique known as ab initio molecular dynamics (AIMD), which combines "on the fly" electronic structure calculations with finite temperature dynamics. In the present work, we have used the ADMP method[46] where the one-electron density matrix is expanded in an atom-centered (Gaussian) basis and propagated as an electronic variable. ADMP employs an extended Lagrangian similar to the well-known Car−Parrinello molecular dynamics. It can treat all electrons quantum-mechanically and can control the deviations from the Born−Oppenheimer surface precisely.

When thermal effects are included through AIMD, the SSCC values involving N-1 decrease slightly, by 0.10−0.13 Hz, while ^2J(N-3,H-4) and ^3J(N-3,H-6) increase by 2.02 and 1.21 Hz, or 43 and 85%, respectively [compare J_e(//B3LYP) and J^{300K}(//AIMD) in Table 1]. Upon going from J^{300K}(//AIMD) to J^{300K}(AIMD/PCM//AIMD), the computed SSCC values change by at most 0.10 Hz, indicating again that they are not influenced much by the continuum model. Larger changes are seen in the model (1w) with one explicit water molecule hydrogen-bonded to N-3; in this case, the SSCC values for ^2J(N-3,H-4) and ^3J(N-3,H-6) increase by 0.64 and 0.31 Hz, respectively, relative to the simulation in vacuo [compare J^{300K}(AIMD(1w))//AIMD(1w)) and (J^{300K}(//AIMD))].

A single solute−solvent cluster in a particular arrangement is clearly an oversimplified description of the real situation of a molecule in solution. We therefore simulated the latter by performing AIMD simulations of **1** embedded in a periodic water box, followed by quantum-mechanical evaluations of the SSCC averaged over snapshots along the trajectory. In the NMR calculations, smaller (non periodical) sections of the full (periodic) system were taken.

Similar approaches using AIMD simulations at the DFT level have been adopted before, for instance, to study the gas-to-liquid shift in water[71,72] or to model transition-metal chemical shifts in aqueous solution.[73−75] The selection of solvent molecules to be included in the NMR computations was done as follows.[20] First, the number of water molecules involved in hydrogen bonds with **1** was determined based on purely geometric criteria, assuming a hydrogen bond if the distance between a N or O atom from **1** and an O atom from water is less than 3.5 Å and the OH bond is directed toward the acceptor atom such that the X—H—O angle is greater than 140°.[33] The resulting average number was 4.8, with minimum and maximum values of 3 and 7, respectively. On average, roughly one water molecule is attached to N-3 and to each of the O atoms from the nitro group, and the alcohol function in the side chain donates and accepts one H-bond (Figure 3). The SSCC values were calculated for a typical snapshot, keeping just the substrate and its H-bonded water molecules. In subsequent calculations, more and more water molecules from the actual snapshot were included, adding them successively according to the shortest distance between the O(water) atom and the center of the imidazole ring. It turned out that the investigated coupling constants of interest did not change significantly when more than seven water molecules in total were present. This number of water molecules was therefore chosen in all 40 snapshots, over which the SSCC values were averaged.[20]

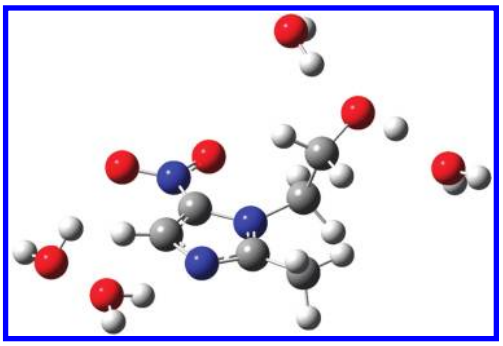

Figure 3. Typical snapshot from an AIMD simulation of **1** in water.

Some of the 40 selected snapshots from the AIMD simulations do not contain a hydrogen bond between the N-3 atom of **1** and a solvent water molecule. When averaging over the SSCC values computed with explicit water molecules for all 40 snapshots, there is an increase of 0.40 and 0.20 Hz for ^2J(N-3,H-4) and ^3J(N-3,H-6), respectively, relative to the results without explicit solvent [compare J^{300K}(//AIMD) and J^{300K}(AIMD(H_2O)//AIMD(H_2O))], which is however less pronounced than that in the case of the cluster with one explicit water molecule at N-3 [see J^{300K}(AIMD(1w))//AIMD(1w)) in Table 1]. Snapshots

with a hydrogen bond between the N-3 atom and a solvent water molecule generally show a higher increase in these SSCC values than those without such a hydrogen bond. It thus appears that the solvent effects on the coupling constants involving N-3 are dominated by hydrogen bonding (see the discussion of the paramagnetic contributions above), most likely by the electrostatic component of the hydrogen bond. The influence of this electrostatic interaction on the NMR scalar coupling constant has previously been discussed in the literature for other coupling pathways.[76−79] The effect of the N···OH hydrogen bond on the ^2J(N-3,H-4) and ^3J(N-3,H-6) couplings can be detected experimentally (an increase of few Hz) and has been attributed to hyperconjugative interactions.[76−78]

Finally, we carried out NMR calculations for the 40 snapshots from the AIMD simulation representing the water solvent by PCM. The average SSCC values with and without explicit water molecules are generally quite similar [see J^{300K}(AIMD(H_2O)//AIMD) and J^{300K}(AIMD(H_2O)/PCM)//AIMD(H_2O)) in Table 1], with deviations of 0.07−0.13 Hz for ^2J(N-3,H-4) and ^2J(N-1,H-7) and 0.05−0.10 Hz for the other couplings. Theoretically, the best accord with the real situation in solution is expected by averaging over a sufficient number of AIMD snapshots and performing NMR calculations that explicitly include discrete water molecules close to the solute and a polarizable dielectric to account for the effects of the bulk solvent[80,81] [AIMD(H_2O)/PCM//AIMD(H_2O)].

It is well-known that the cavity definition in continuum solvation methods can have a large impact on the computed properties. Previous work has shown that solvent effects are amplified for smaller cavities.[20] As expected, the ^{15}N NMR parameters are more strongly influenced by cavity size than the ^{13}C and ^{1}H NMR parameters. The PCM results may thus be associated with a notable uncertainty when the lone pair at nitrogen is located close to the PCM surface.

Regarding the SSCC involving the N-3 nucleus, the most affected by solvent and thermal effects, we can observe that methodologies, such as J^{300K}(AIMD(H_2O)//AIMD), J^{300K}(AIMD(H_2O)/PCM)//AIMD(H_2O)), and J^{300K}(AIMD(1w))//AIMD(1w), lead to the best agreement with the experimental data.

A deeper analysis of Table 1 reveals that the highest deviation between theory and experiment was about 1.95 and 0.72 Hz for the coupling constants ^2J(N-3,H-4) and ^3J(N-1,H-6), respectively. Whereas high accuracy between the experimental and theoretical data at the DFT level of calculation for this kind of coupling is difficult to obtain due to the lack of exact Hartree−Fock exchange in some functional, our theoretical predictions reproduce the exact observed trend. For instance, for ^2J(N-1,H-8), a deviation of 0.35 Hz is obtained, while for ^2J(N-1,H-4) and ^3J(N-3,H-6), deviations of just 0.27 and 0.26 Hz are observed. In addition, as predicted by theoretical calculation, the ^3J(NO_2,H-4) was not also detected using HR-HMBC techniques. This result reinforces the previous conclusion on the very small coupling between the nitro group and hydrogen nuclei at the imidazole ring (below 1 Hz). Interestingly, a slight increase in the deviation between theory and experiment was obtained for approaches involving PCM-type continuum models.

Due to conformational fluctuations from MD simulations, the average SSCC values are obtained with variable precision, reflected by the standard deviation of the mean, which we from now on call "the error bar" (Table 1). It is important to note that the error bars for ^2J(N-3,H-4) and ^3J(N-3,H-6) were 0.64 and 0.29 [J^{300K}(//AIMD)]; 0.65 and 0.23 [J^{300K}(AIMD/(PCM)//AIMD)], 0.68 and 0.27 [J^{300K}(AIMD(1w))//AIMD(1w))]; 0.61 and 0.19 [J^{300K}(AIMD(H2O)//AIMD(H_2O))]; and finally 0.63 and 0.21 Hz [J^{300K}(AIMD(H_2O)/PCM//AIMD(H_2O))]. The deviation (relative error) between theoretical and experimental results decreased significantly when we introduced the fluctuation on SSCC from MD results. In this way, the AIMD simulations give good agreement with hydrogen bond geometries and SSCC, indicating proper description of the conformational space in solution explored by MD data. A more realistic scenario is obtained when both discrete water molecules and the dielectric are included, as pointed out previously.[82,83] It is well-known that the AIMD simulations in water offer a reasonable description of the structure and dynamics of the solution, with the hydrogen bonds between solute and solvent molecules being treated quantum-mechanically.[20,84] Furthermore, in the AIMD framework, the quantum treatment of both solvent and solute may cause changes in the hyperconjugative interactions and coupling pathways compared with the situation in the isolated solute molecule. To gain a better understanding of these phenomena, we carried out NBO calculations and analyzed the hyperconjugative interactions present in the imidazole ring.

3.3. Nonbonded Interactions versus Solvation Models. It is well-known that nonbonded hyperconjugative interactions can affect NMR parameters such as SSCC.[29,85] They also play an important role in structural chemistry.[86−88] Other studies highlight their strong influence on the kinetics and thermodynamics of organic[89] and inorganic[90,91] molecules in solution. From our calculations, as expected, the Fermi contact (FC) term modulates the coupling ^nJ(N,H) in the imidazole ring. For ^3J(N-1,H-4), on average, this term is responsible for 85.17% of the coupling value, while other contributions, such as spin−dipolar (SD), paramagnetic spin−orbit (PSO), and diamagnetic spin−orbit (DSO) are responsible for 1.15, 5.63, and 8.05%, respectively. It is important to mention that the use of basis sets that can reproduce the electronic density in the nuclear region is particularly important when calculating the FC term.

In the area of NMR spectroscopy, electronic perturbations have been identified that can reduce coupling pathways,[19,29] in particular, hyperconjugative interactions $\sigma_{CH} \rightarrow \pi^*$ and $\pi \rightarrow \sigma_{CH}^*$ that involve the coupling nucleus (H). These two interactions are commonly accepted to provide the main transmission mechanism for the FC term of long-range benzylic-type couplings.[78,92] We carried out a NBO analysis using second-order perturbation theory to quantify the hyperconjugative interactions in the imidazole ring of **1** and to monitor the solvent effects on the interaction energies. The latter are dependent on the energies of the interacting orbitals, which also influence the magnetic coupling strength, and one may hence expect correlations between the NBO interaction energies and the ^nJ(N,H) SSCC values.

The results of the NBO analysis are reported in Tables 3 and 4 for the various computational approaches applied presently (static and dynamic calculations, without or with explicit solvent molecules or with continuum solvation). The computed orbital interaction energies range over 2.05−2.32, 2.21−3.64, 1.10−1.37, and 1.32−1.84 kcal mol^{-1} for $\pi_{N\text{-}1C\text{-}5} \rightarrow \sigma^*_{CH\text{-}4}$, $\pi_{N\text{-}3C\text{-}2} \rightarrow \sigma^*_{CH\text{-}4}$, $\pi_{C\text{-}5C\text{-}4} \rightarrow \sigma^*_{CH\text{-}4}$, and $n_{N\text{-}3} \rightarrow \sigma^*_{CH\text{-}4}$ (Table 3) and over 2.94−3.13, 2.28−2.32, and 2.82−3.08 kcal mol^{-1} for $\sigma_{CH\text{-}4} \rightarrow \pi^*_{N\text{-}1C\text{-}5}$, $\sigma_{CH\text{-}4} \rightarrow \pi^*_{N\text{-}3C\text{-}2}$, and $\sigma_{CH\text{-}4} \rightarrow \pi^*_{C\text{-}5C\text{-}4}$ (Table 4), respectively. Looking at the individual values for a given interaction, the highest orbital interaction energies are generally

Table 3. Orbital Interaction Energies [kcal mol^{-1}] for the Hyperconjugative Interaction to the σ^*_{CH} Antibond of Metronidazole (1)

level of approximation[a]	$\pi_{N\text{-}1C\text{-}5} \rightarrow \sigma^*_{CH\text{-}4}$	$\pi_{N\text{-}3C\text{-}2} \rightarrow \sigma^*_{CH\text{-}4}$	$\pi_{C\text{-}5C\text{-}4} \rightarrow \sigma^*_{CH\text{-}4}$	$n_{N\text{-}3} \rightarrow \sigma^*_{CH\text{-}4}$
J_e(//B3LYP)	2.17	3.64	1.16	1.84
J_e(PCM//B3LYP/PCM)	2.14	2.28	1.14	1.78
J_e(B3LYP(1w))//B3LYP(1w))	2.05	2.21	1.10	1.32
J^{300K}(//AIMD)	2.32	3.50	1.37	1.75
J^{300K}(AIMD/PCM)//AIMD)	2.30	3.38	1.34	1.70
J^{300K}(AIMD(1w))//AIMD(1w))	2.27	3.37	1.32	1.65
J^{300K}(AIMD(H_2O)//AIMD(H_2O)[b])	2.21	3.18	1.33	1.52
J^{300K}(AIMD(H_2O)[b]/PCM//AIMD(H_2O)[b])	2.27	3.27	1.30	1.50

[a] Notation: level of chemical shift computation//level of geometry optimization or MD simulation. [b] Section from the full solution containing seven water molecules explicitly (see text).

Table 4. Orbital Interaction Energies [kcal mol^{-1}] for the Hyperconjugative Interaction from the $\sigma_{CH\text{-}4}$ Bond of Metronidazole (1)

level of approximation[a]	$\sigma_{CH\text{-}4} \rightarrow \pi^*_{N\text{-}1C\text{-}5}$	$\sigma_{CH\text{-}4} \rightarrow \pi^*_{N\text{-}3C\text{-}2}$	$\sigma_{CH\text{-}4} \rightarrow \pi^*_{C\text{-}5C\text{-}4}$
J_e(//B3LYP)	3.09	3.32	3.02
J_e(PCM//B3LYP/PCM)	3.01	3.19	2.93
J_e(B3LYP(1w))//B3LYP(1w))	2.95	3.02	2.84
J^{300K}(//AIMD)	3.13	2.66	3.08
J^{300K}(AIMD/PCM)//AIMD)	3.08	2.48	2.94
J^{300K}(AIMD(1w))//AIMD(1w))	3.01	2.35	2.87
J^{300K}(AIMD(H_2O)//AIMD(H_2O)[b])	3.07	2.30	2.82
J^{300K}(AIMD(H_2O)[b]/PCM//AIMD(H_2O)[b])	2.94	2.28	2.99

[a] Notation: level of chemical shift computation//level of geometry optimization or MD simulation. [b] Section from the full solution containing seven water molecules explicitly (see text).

found for the isolated molecule, and the lowest ones are found when explicit solvent molecules are included, with the PCM-based results being intermediate (both in the static and the dynamic calculations). To quote some specific example, we compare dynamics calculations without and with explicit solvent water molecules [see J^{300K}(//AIMD) and J^{300K}(AIMD(H_2O)//AIMD(H_2O) in Tables 3 and 4)], where we observe a decrease of the hyperconjugative interactions in solution by 0.32 and 0.36 kcal mol^{-1} for $\pi_{N\text{-}3C\text{-}2} \rightarrow \sigma^*_{CH\text{-}4}$ and $\sigma_{CH\text{-}4} \rightarrow \pi^*_{N\text{-}3C\text{-}2}$, respectively, which correlates with a significant increase of 0.4 Hz in the corresponding SSCC value (Table 1). The same qualitative behavior is generally seen for all types of computational approaches used presently. The inclusion of solvent thus reduces the hyperconjugative interactions, in general, and, in particular, those involving the $\sigma_{CH\text{-}4}$ bond and the $\sigma^*_{CH\text{-}4}$ antibond (with the coupling nucleus H-4), both at the PCM level this is reduced even more so with explicit solvent. Hence, solvent effects can indeed affect hyperconjugative interactions and coupling pathways in solute molecules.

The inverse relation between the NBO interaction energies (Tables 3 and 4) and the computed SSCC values (Table 1) provides some rationalization for the observation that the solvent effects on the SSCC are more pronounced in an explicit solvent representation (compared with PCM-type continuum models). This raises the question whether specific hydrogen bonds are

Table 5. AIM Parameters [au] of the Bond Critical Points between 1 and Solvent Water

level of approximation[a]	ρ_b	$\nabla^2\rho_b$	ε	H
J_e(B3LYP(1w))//B3LYP(1w))	0.031	0.042	0.045	0.001
J^{300K}(AIMD(1w))//AIMD(1w))	0.019	0.046	0.040	0.002
J^{300K}(AIMD(H_2O)//AIMD(H_2O)[b])	0.020	0.052	0.045	0.001
J^{300K}(AIMD(H_2O)[b]/PCM//AIMD(H_2O)[b])	0.017	0.045	0.064	0.003

[a] Notation: level of chemical shift computation//level of geometry optimization or MD simulation. [b] Section from the full solution containing seven water molecules explicitly (see text).

responsible for this distinction. Classically, hydrogen bonds are thought to arise from the electrostatic interaction of a positively charged H atom and an electronegative atom X (usually F, O, and N).[93] However, electronic delocalization between solute and solvent molecules may also occur and lead to a partially covalent character for such bonds.[94−96] It is generally assumed that the classical contributions to hydrogen bonding can be treated by continuum solvation models as long as the interaction between solute and solvent is moderately polar.[40,70] Such models[39−42] are widely used today and have often been applied with success.[97] On the other hand, it is also clear that the electronic effects of specific interactions between solute and solvent are better evaluated by inclusion of explicit solvent molecules.[20,80,81] This applies in particular to solvent molecules in the first coordination shell with strong and specific solute−solvent interactions that cannot be considered in a continuum model.[80]

In order to shed some more light on the specific interactions between metronidazol (1) and solvent molecules, we have performed AIM calculations.[54] It is known[98,99] that fairly good linear correlations exist between the charge densities at the BCPs of hydrogen bonds and their properties. We have used the computed DFT densities to perform an AIM analysis and to locate the BCPs for the relevant hydrogen bonds in the N···HO region. The results are summarized in Table 5.

The electronic density (ρ_b) at the BCP relates to the bond strength. It is rather low and reduced from the static value of 0.031 au [J_e(B3LYP(1w))//B3LYP(1w)) in Table 5] to 0.017−0.020 au in the dynamics calculations that include thermal effects [see, e.g., J^{300K}(AIMD(1w))//AIMD(1w))]. Negative values of the Laplacian ($\nabla^2\rho_b$) at the BCP signify charge concentration and hence covalent bonding, while positive values indicate charge depletion, with electron density being moved from the BCP region toward the atomic basins (closed-shell interactions, typical of highly

Table 6. CHELPG Charges [e] for Atoms Present in the Imidazole Ring

level of approximation[a]	N-1	C-2	N-3	C-4	C-5
J_e(//B3LYP)	−0.16	0.49	−0.52	0.09	−0.06
J_e(PCM//B3LYP/PCM)	−0.15	0.52	−0.57	0.10	−0.05
J_e(B3LYP(1w))//B3LYP(1w))	−0.06	0.37	−0.46	0.14	0.37
J^{300K}(//AIMD)	−0.16	0.49	−0.52	0.09	−0.06
J^{300K}(AIMD/PCM)//AIMD)	−0.17	0.50	−0.56	0.10	−0.07
J^{300K}(AIMD(1w))//AIMD(1w))	−0.09	0.48	−0.49	0.12	−0.10
J^{300K}(AIMD(H_2O)//AIMD(H_2O)[b])	−0.10	0.37	−0.42	0.13	−0.12
J^{300K}(AIMD(H_2O)[b]/PCM//AIMD(H_2O)[b])	−0.05	0.42	−0.52	0.14	−0.15

[a] Notation: level of chemical shift computation//level of geometry optimization or MD simulation. [b] Section from the full solution containing seven water molecules explicitly (see text).

ionic bonds). In the present case, the computed $\nabla^2\rho_b$ values (Table 5) are all positive and within the range expected for normal hydrogen bonds,[100,101] thus confirming the predominantly electrostatic character of the hydrogen bond between N-3 and the solvent water molecule.

Atomic charges may be determined by fitting the molecular electrostatic potential (MEP) around a given molecule. Such CHELPG charges are listed in Table 6 for the atoms N-1, C-2, N-3, C-4, and C-5 in the imidazole ring. The computed charges for N-3 are most negative, ranging from −0.42 e to −0.57 e, consistent with the electrostatic character of the hydrogen bond between N-3 and water. Explicit inclusion of the hydrogen-bonded water molecule in the DFT calculation lowers the charge at N-3 somewhat in absolute value (Table 6).

The hydrogen bond between N-3 and water might allow for some charge transfer toward the water molecule, leading to an increase in the discussed couplings [^2J(N-3,H-4) and ^3J(N-3,H-6)]. This conclusion is in agreement with previous work, showing an increase in the one-bond J(N,H) coupling constant if there is a predominantly electrostatic hydrogen bond involving the nitrogen atom.[56,78,102−105]

To summarize, our results highlight the impact of thermal and solvent effects on SSCC. For instance, when going from static equilibrium to thermally averaged SSCC values, ^2J(N-3,H-4) and ^3J(N-3,H-6) change by 47 and 85%, respectively [compare J_e(//B3LYP) and J^{300K}(//AIMD) in Table 1]. Likewise, the static SSCC values in vacuo and in solution differ by 45 and 77% for ^2J(N-3,H-4) and ^3J(N-3,H-6), respectively [compare J_e(//B3LYP) and J_e(PCM//B3LYP/PCM) in Table 1]. These effects are largest for the coupling constants involving N-3 that is hydrogen bonded to a solvent water molecule. They are captured with all computational solvation models applied (including PCM, microsolvated clusters, and MD snapshots with explicit water solvent), which thus provides a qualitatively consistent picture (albeit with some quantitative differences). In fact, a better agreement between theory and experiment was obtained with inclusion of solvent and thermal effects.

In solution, the transmission of the spin information between H-4 and N-3 is perturbed by the effects of hydrogen bonding with solvent molecules, which are primarily electrostatic in character. Apparently, the PCM model reproduces the effects of such hydrogen bonds on NMR SSCC reasonably well (Table 1), as noted before,[15,104] despite the fact that continuum behavior is not expected at small distances from the solute molecule.[80,81] From a theoretical point of view, a proper understanding of solvation is best achieved by the combined use of discrete and continuum models, where the specific interactions between solute and nearby solvent molecules are treated explicitly at the quantum level and the distant bulk solvent is represented by a polarizable continuum. This approach takes into account both the electrostatic and delocalization effects, which are both known to affect SSCC.[19]

4. CONCLUSIONS

Hydrogen bonds in liquids can be of crucial importance for solvent effects in spectroscopy. In this work, thermal and solvent effects on the SSCCs of metronidazole (**1**) were studied computationally with appropriate quantum-chemical methods. Metronidazole may serve as a model compound to investigate the influence of solvent molecules on the NMR SSCC in heterocyclic rings. We find a hydrogen bond between **1** and a solvent water molecule that is associated with a bond critical point between the imidazole N-3 atom and a water H atom. AIM analysis indicates this hydrogen bond to be mainly electrostatic in nature. Simple static SSCC calculations in vacuo underestimate the ^nJ(N-3,H) coupling constants because of the neglect of hydrogen bonding. PCM-based treatments perform reasonably well because of the electrostatic character of the hydrogen bond. For more reliable predictions, it is important to take into account the dynamics of the system and to include nearby solvent molecules explicitly.

The reduction of the hyperconjugative interactions involving the σ_{CH} bond or the σ^*_{CH} antibond (with the coupling nucleus H) that is found in solution appears to be correlated to the reduction of coupling pathways in the imidazole ring. Because nuclear spin orientation information is transferred electronically to the other nuclei in the molecule, experimentally determined J-couplings directly reflect the nature of the chemical bond involved.[106−109] Unlike most other NMR properties, which can be understood on the basis of semiclassical physics, J-coupling is a purely quantum-mechanical phenomenon. The present results provide evidence that hyperconjugative effects in solute molecules are not due to changes in geometric parameters upon solvation but arise from the direct response of the electronic wave function to the presence of the solvent, which can be represented by discrete molecules and/or the dielectric bulk. We believe that our findings may be helpful to rationalize the relation between NMR parameters and the interactions in hydrogen-bonded complexes. Further applications along these lines are in progress.

AUTHOR INFORMATION

Corresponding Author

*E-mail: teo@dqi.ufla.br. Fax: 55 35 3829-1271. Tel: 55 35 3829-1522.

■ ACKNOWLEDGMENT

We are grateful to the Brazilian agencies CAPES and FAPEMIG and also the German agency DAAD for funding part of this work. T.C.R. wishes to thank CNPq for the fellowship and the financial support provided. Finally, we would like to thank the Dr. Christophe Fares and Ms. C. Wirtz for recording and interpretation of the NMR spectra and for helpful discussions during their analysis.

■ REFERENCES

(1) Morel, C. M. *Parasitol. Today* **2000**, *16*, 522–525.
(2) Romero, E. L.; Morilla, M. J. *Adv. Drug Delivery Rev.* **2010**, *62*, 576–588.
(3) Kayama, H.; Takeda, K. *Microbes Infect.* **2010**, *12*, 511–517.
(4) Trouiller, P.; Olliaro, P.; Torreele, E.; Orbinski, J.; Laing, R.; Ford, N. *Lancet* **2002**, *359*, 2188–2194.
(5) da Cunha, E. F. F.; Ramalho, T. C.; Mancini, D. T.; Fonseca, B. E. M.; Oliveira, A. A. *J. Braz. Chem. Soc.* **2010**, *21*, 1787–1806.
(6) Bost, F.; Jacobs, R. T.; Kowalczyk, P. *Curr. Opin. Drug Discovery Dev.* **2010**, *13*, 286–296.
(7) Brown, J. M. *Cancer Res.* **1999**, *59*, 5863–5867.
(8) Hori, H; Nagasawa, H.; Terada, H. *Advances in Environmental Science and Technology: Oxidants in the Environment*; Nriagu, J. O., Simmons, M. S., Eds.; John Wiley: New York, 1994; Vol. 28, pp 425−443.
(9) Viodé, C.; Bettache, N. *Biochem. Pharmacol.* **1999**, *57*, 549–556.
(10) Nussbaum, K.; Honek, J.; Cadmus, C. M. C. V.; Efferth, T. *Curr. Med. Chem.* **2010**, *17*, 1594–1617.
(11) Lauffer, R. B. *Chem. Rev.* **1987**, *87*, 901–927.
(12) Anderson, C. J.; Welch, M. J. *Chem. Rev.* **1999**, *99*, 2219–2234.
(13) McCoy, C. L.; McIntyre, D. J. O.; Robinson, S. P.; Aboagye, E. O.; Griffiths, J. R. *Br. J. Cancer* **1996**, *74*, S226–S231.
(14) Ali, H.; van Lier, J. E. *Chem. Rev.* **1999**, *99*, 2379–2450.
(15) Dracinsky, M; Bour, P. *J. Chem. Theory Comput.* **2010**, *6*, 288–299.
(16) Bermel, W.; Bertini, I.; Felli, I. C.; Peruzzini, R.; Pierattelli, R. *ChemPhysChem* **2010**, *11*, 689–695.
(17) Helgaker, T.; Jaszunski, M.; Pecul, M. *Prog. Nucl. Magn. Res. Spectrosc.* **2008**, *53*, 249–268.
(18) Jensen, F. *Theor. Chem. Acc.* **2010**, *126*, 371–382.
(19) Contreras, R. H.; Gotelli, G.; Ducati, L. C.; Barbosa, T. A.; Tormena, C. F. *J. Phys. Chem. A* **2010**, *114*, 1044–1051.
(20) Ramalho, T. C.; Bühl, M. *Magn. Reson. Chem.* **2005**, *43*, 139–146.
(21) Schreckenbach, G. *Inorg. Chem.* **2002**, *41*, 6560–6572.
(22) Ziegler, T. *Chem. Rev.* **1991**, *91*, 651–667.
(23) Siuda, P.; Sadlej, J. *J. Phys. Chem. A* **2011**, *115*, 612–619.
(24) Taha, H. A. *J. Chem. Theory Comput.* **2010**, *6*, 212–218.
(25) Costa, F. L. P.; de Albuquerque, A. C. F.; dos Santos, F. M.; de Amorim, M. B. *J. Phys. Org. Chem.* **2010**, *23*, 972–977.
(26) Autschbach, J.; Le Guennic, B. *J. Chem. Educ.* **2007**, *84*, 156–171.
(27) Vaara, J.; Jokisaari, J.; Wasylishen, R. E.; Bryce, D. L. *Prog. Nucl. Magn. Reson. Spectrosc.* **2002**, *41*, 233–304.
(28) Helgaker, T.; Jaszunski, M.; Pecul, M. *Prog. Nucl. Magn. Reson. Spectrosc.* **2008**, *53*, 249–268.
(29) Contreras, R. H.; Peralta, J. E. *Prog. Nucl. Magn. Reson. Spectrosc.* **2000**, *37*, 321–425.
(30) Bifulco, G.; Dambruoso, P.; Gomez-Paloma, L.; Riccio, R. *Chem. Rev.* **2007**, *107*, 3744–3779.
(31) Boehr, D. D.; Dyson, H. J.; Wright, P. E. *Chem. Rev.* **2006**, *106*, 3055–3079.
(32) Helgaker, T.; Jaszunski, M.; Ruud, K. *Chem. Rev.* **1999**, *99*, 293–352.
(33) Geethalakshmi, K. R.; Waller, M. P.; Thiel, W.; Bühl, M. *J. Phys. Chem. B* **2009**, *113*, 4456–4465.
(34) Ramalho, T. C.; de Alencastro, R. B.; Figueroa-Villar, J. D. *Biophys. Chem.* **2004**, *110*, 267–291.
(35) Tiana, S. X.; Yang, J. *J. Chem. Phys.* **2007**, *126*, 141103–141107.
(36) Becke, A. D. *J. Chem. Phys.* **1993**, *98*, 5648.
(37) Lee, C.; Yang, W.; Parr, R. G. *Phys. Rev. B* **1988**, *37*, 785–89.
(38) Cheeseman, J. R.; Trucks, G. W.; Keith, T. A.; Frisch, M. J. *J. Chem. Phys.* **1996**, *104*, 5497–5505.
(39) Cances, T. M.; Mennucci, B.; Tomasi, J. *J. Chem. Phys.* **1997**, *107*, 3032–3039.
(40) Barone, V.; Cossi, M.; Tomasi, J. *J. Comput. Chem.* **1998**, *19*, 404–410.
(41) Cossi, M.; Barone, V.; Mennucci, B.; Tomasi, J. *Chem. Phys. Lett.* **1998**, *286*, 253–258.
(42) Cossi, M.; Scalmani, G.; Rega, N.; Barone, V. *J. Chem. Phys.* **2002**, *117*, 43–49.
(43) Calva-Tejada, N.; Bernes, S.; Castillo-Blum, S. E.; Noth, H.; Vicente, R.; Barba-Behren, N. *J. Inorg. Biochem.* **2002**, *91*, 339–345.
(44) Iyengar, S. S.; Schlegel, H. B.; Millam, J. M.; Voth, G. A.; Scuseria, G. E.; Frisch, M. J. *J. Chem. Phys.* **2001**, *115*, 10291–302.
(45) Van der Spoel, D.; Van Buuren, A. R.; Apol, E.; Meulenhoff, P. J.; Tieleman, D. P.; Sijbers, A. L. T. M.; Hess, B.; Feentra, A. K.; Lindahl, E.; Van Drunen, R.; Berendsen, H. J. C. *GROMACS user manual version 3.0*; University of Groningen, Department of Biophysical Chemistry: Groningen, The Netherlands, 2001.
(46) Schlegel, H. B.; Iyengar, S. S.; Li, X.; Millam, J. M.; Voth, G. A.; Scuseria, G. E.; Frisch, M. J. *J. Chem. Phys.* **2002**, *117*, 8694–704.
(47) Ramalho, T. C.; Bühl, M.; de Alencastro, R. B.; Figueroa-Villar, J. D. *Helv. Chim. Acta* **2005**, *88*, 2705–2721.
(48) Ditchfield, R. *Mol. Phys.* **1974**, *27*, 789–798.
(49) Wolinski, K.; Hinton, J. F.; Pulay, P. *J. Am. Chem. Soc.* **1990**, *112*, 8251–8258.
(50) Cheeseman, J. R.; Trucks, G. W.; Keith, T. A.; Frisch, M. J. *J. Chem. Phys.* **1996**, *104*, 5497–5507.
(51) Dransk, M.; Kaminsk, J.; Bour, P. *J. Phys. Chem. B* **2009**, *113*, 14698–14707.
(52) Jaworska, M.; Hrynczyszyn, P. B.; Welniak, M.; Wojtczak, A.; Nowicka, K.; Krasinski, G.; Kassassir, H.; Ciesielski, W.; Potrzebowski, M. *J. Phys. Chem. A* **2010**, *114*, 12522–12530.
(53) Frisch, M. J.; Trucks, G. W.; Schlegel, H. B.; Scuseria, G. E.; Robb, M. A.; Cheeseman, J. R.; Montgomery, Jr., J. A.; Vreven, T.; Kudin, K. N.; et al. *Gaussian 03*, revision C.02; Gaussian, Inc.: Wallingford, CT, 2004.
(54) Bader, R. F. W. *Atoms in Molecules: A Quantum Theory*; Clarendon Press: Oxford, U.K., 1990.
(55) Popelier, P. L. A.; Aicken, F. M.; O'Brien, S. E. *Chemical Modelling: Applications and Theory*; Royal Society of Chemistry: London, 2000; Vol. 1, Chapter 3, p 143.
(56) Cioslowski, J.; Mixon, S. T. *J. Am. Chem. Soc.* **1991**, *113*, 4142–4150.
(57) Kosov, D. S.; Popelier, P. L. A. *J. Phys. Chem. A* **2000**, *104*, 7339–7348.
(58) Ángyán, J. G.; Loos, M.; Mayer, I. *J. Phys. Chem.* **1991**, *98*, 5244–5253.
(59) Toledo, E. J. L.; Custodio, R.; Ramalho, T. C.; Porto, M. E. G.; Magriotis, Z. M. *J. Mol. Struct.: THEOCHEM* **2009**, *915*, 170–177.
(60) Wang, P.; Zhang, Y. L.; Streitwieser, A. *J. Am. Chem. Soc.* **1991**, *113*, 55–64.
(61) Keith, T. A. *AIMAll*, version 090423; 2009.
(62) Breneman, C. M.; Wiberg, K. B. *J. Comput. Chem.* **1990**, *11*, 361–373.
(63) Furihata, K.; Tashiro, M.; Seto, H. *Magn. Reson. Chem.* **2011**, *39*, 53–58.
(64) Silvestri, R.; Artico, M.; Marceddu, S. T.; DeMontis, F.; LaColla, P. *Bioorg. Med. Chem. Lett.* **2000**, *10*, 253–258.
(65) Ernst, R. R.; Bodenhausen, G. Principles of Nuclear Magnetic. *Resonance in One and Two Dimensions*; Clarendon Press: Oxford, U.K., 1987.
(66) Barone, V.; Cossi, M.; Tomasi, J. *J. Comput. Chem.* **1998**, *19*, 404–415.
(67) Kutzelnigg, W.; Fleischer, U.; Schindler, M. *NMR Basic Principles and Progress*; Springer: Berlin, Germany, 1990; Vol. 23, p 165.
(68) Cances, E.; Mennucci, B.; Tomasi, J. *J. Chem. Phys.* **1997**, *107*, 3032–3041.

(69) Barone, V.; Improta, R.; Rega, N. *Acc. Chem. Res.* **2008**, *41*, 605–616.
(70) Tomasi, J. *Theor. Chem. Acc.* **2004**, *112*, 184–203.
(71) Malkin, V. G.; Malkina, O. L.; Steinebrunner, G.; Huber, H. *Chem.—Eur. J.* **1996**, *2*, 452–459.
(72) Murugan, N. A.; Rinkevicius, Z.; Agren, H. *J. Phys. Chem. A* **2009**, *113*, 4833–4839.
(73) Bühl, M.; Schurhammer, R.; Imhof, P. *J. Am. Chem. Soc.* **2004**, *126*, 3310–3318.
(74) Waller, M. P.; Bühl, M.; Geethalakshmi, K. R.; Wang, D.; Thiel, W. *Chem.—Eur. J.* **2007**, *13*, 4723–4732.
(75) Bühl, M.; Thiel, W. *Inorg. Chem.* **2004**, *43*, 6377–6382.
(76) Contreras, R. H.; Provasi, P. F.; dos Santos, F. P.; Tormena, C. F. *Magn. Reson. Chem.* **2009**, *47*, 113–120.
(77) Neto, A. C.; dos Santos, F. P.; Contreras, R. H.; Rittner, R.; Tormena, C. F. *J. Phys. Chem. A* **2008**, *112*, 11956–11959.
(78) Contreras, R. H.; Esteban, A. L.; Diez, E.; Della, E. W.; Lochert, I. J.; dos Santos, F. P.; Tormena, C. F. *J. Phys. Chem. A* **2006**, *110*, 4266–4275.
(79) Tormena, C. F.; Rittner, R.; Contreras, R. H.; Peralta, J. E. *J. Phys. Chem. A* **2004**, *108*, 7762–7768.
(80) Pliego, J. R.; Riveros, J. M. *J. Phys. Chem. A* **2001**, *105*, 7241–7247.
(81) Pliego, J. R. *J. Phys. Chem. B* **2009**, *113*, 505–510.
(82) Hemmingsen, L.; Amara, P.; Ansorborlo, E.; Field, M. J. *J. Phys. Chem. A* **2000**, *104*, 4095–4101.
(83) Real, F.; Trumm, M.; Vallet, V.; Schimmelpfennig, B.; Masella, M.; Flament, J.-P. *J. Phys. Chem. B* **2010**, *114*, 15913–15924.
(84) Dracinsky, M.; Kaminsky, J.; Bour, P. *J. Phys. Chem. B* **2009**, *113*, 14698–14707.
(85) Krivdin, L. B.; Contreras, R. H. *Annu. Rep. NMR Spectrosc.* **2007**, *61*, 133–245.
(86) Guru Row, T. N.; Parthasarathy, R. *J. Am. Chem. Soc.* **1981**, *103*, 477–479.
(87) Wang, X.; Houk, K. N.; Spichty, M.; Wirth, T. *J. Am. Chem. Soc.* **1999**, *121*, 8567–8576.
(88) Rosenfield, R. E.; Pathasatathy, R. *J. Am. Chem. Soc.* **1977**, *99*, 4860–4899.
(89) Ramalho, T. C.; Martins, T. L. C.; Borges, L. E. P; Figueroa-Villar, J. D. *Int. J. Quantum Chem.* **2003**, *95*, 267–273.
(90) Ramalho, T. C.; Oliveira, L. C. A.; Carvalho, K. T. G.; Souza, E. F.; da Cunha, E. F. F.; Nazzaro, M. *Mol. Phys.* **2009**, *107*, 171–179.
(91) La Porta, F. A.; Ramalho, T. C.; Santiago, R. T.; Rocha, M. V. J.; da Cunha, E. F. F. *J. Phys. Chem. A* **2011**, *115*, 824–833.
(92) Barfield, M.; Chakrabarti, B. *Chem. Rev.* **1969**, *69*, 757–778.
(93) Steiner, T.; Saenger, W. *Acta Crystallogr., Sect. A* **1993**, *49*, 379–384.
(94) Rankin, K. N.; Boyd, R. J. *J. Comput. Chem.* **2001**, *22*, 1590–1597.
(95) Senthilkumar, L.; Ghanty, T. K.; Ghosh, S. K.; Kolandaivel, P. *J. Phys. Chem. A* **2006**, *110*, 12623–12628.
(96) Chermahini, A. N.; Mohaddeli, A.; Teimouri, A. *Struct. Chem.* **2010**, *21*, 643–649.
(97) Tomasi, J.; Mennucci, B.; Cammi, R. *Chem. Rev.* **2005**, *105*, 2999–3093.
(98) Bader, R. F. W. *J. Phys. Chem. A* **2008**, *112*, 13717–13726.
(99) Merino, G.; Vela, A.; Heine, T. *Chem. Rev.* **2005**, *105*, 3812–3841.
(100) Taylor, R.; Kennard, O. *J. Am. Chem. Soc.* **1982**, *104*, 5063–5070.
(101) Freitas, M. P.; Tormena, C. F.; Rittner, R.; Abraham, R. J. *J. Phys. Org. Chem.* **2003**, *16*, 27–33.
(102) Bakulin, A. A.; Maxim, S. *J. Phys. Chem. A* **2011**, *115*, 1821–1829.
(103) Afonin, A. V.; Ushakov, I. A.; Vashchenko, A. V.; Kondrashov, E. V.; Rulev, A. Y. *Magn. Reson. Chem.* **2010**, *9*, 661–670.
(104) Taurian, O. E.; De Kowalewski, D. G.; Perez, J. E.; Contreras, R. H. *J. Mol. Struct.* **2005**, *754*, 1–9.
(105) Zarzycki, P.; Rustad, J. R. *J. Phys. Chem. A* **2009**, *113*, 291–297.
(106) Wilkens, S. J.; Westler, W. M.; Markley, J. L.; Weinhold, F. *J. Am. Chem. Soc.* **2001**, *123*, 12026–12036.
(107) Murugan, N. A.; Kongsted, J.; Rinkevicius, Z.; Aidas, K.; Agren, H. *J. Phys. Chem. B* **2010**, *114*, 13349–13357.
(108) Ramalho, T. C.; da Cunha, E. F. F; de Alencastro, R. B. *J. Phys.: Condens. Matter* **2004**, *16*, 6159–6170.
(109) Li, H. F.; Zhang, L. B.; Han, L.; Sun, W. M.; Bu, Y. X. *J. Comput. Chem.* **2011**, *32*, 1159–1169.